42nd AIAA Fluid Dynamics Conference and Exhibit
25 - 28 June 2012, New Orleans, Louisiana

AIAA 2012-2968

Analysis of biplane flapping flight with tail

W.B Tay[1], H. Bijl[2] and B.W. van Oudheusden[3]
Faculty of Aerospace Engineering, Delft University of Technology, Kluyverweg 1, 2629 HS Delft, The Netherlands

Numerical simulations have been performed to examine the interference effects between an upstream flapping biplane airfoil arrangement and a downstream stationary tail at a Reynolds number of 1000, which is around the regime of small flapping micro aerial vehicles. The objective is to investigate the effect of the relative distance and angle of attack between the airfoils and its tail on the overall propulsive efficiency, thrust and lift. An immersed boundary method Navier-Stokes solver is used for the simulation. Results show that overall efficiency and average thrust per airfoil can be increased up to 17% and 126% respectively when the top and bottom airfoils come into contact during flapping. When placing the tail at a strategic position, the overall configuration generates much higher lift, although at the expense of decreased efficiency and thrust. Increasing the angle of attack of the tail also helps to increase the lift. Analysis of the vorticity plots reveals the interaction between the vortices and the airfoils and the reason behind the high thrust and lift. The results obtained from this study can be used to optimize the performance of small flapping MAVs.

Nomenclature

c	=	airfoil chord
C_d	=	drag coefficient
C_l	=	lift coefficient
$\overline{C_l}$	=	average lift coefficient
C_t	=	thrust coefficient
$\overline{C_t}$	=	average thrust coefficient
f	=	frequency, Hz
fc	=	external body force
h	=	instantaneous heaving position
h_0	=	heaving amplitude, nondimensionalized by airfoil chord
I_p	=	performance index defined to determine the overall performance of the tandem airfoils
k	=	reduced frequency fc / U_∞
L	=	lift force
M	=	moment created by the lift and drag forces at the pitching axis
p	=	pressure, nondimensionalized by ρU_∞
P_{in}	=	nondimensonal power input
$\overline{P_{in}}$	=	nondimensonal average power input
P_{out}	=	nondimensonal power output
$\overline{P_{out}}$	=	nondimensonal average power output
Re	=	Reynolds number $U_\infty c / \upsilon$
St	=	Strouhal number fh_0 / U_∞
t	=	nondimensionalized time
t_0	=	time when flapping starts

[1] Postdoctoral researcher, Faculty of Aerospace Engineering, Delft University of Technology, Member AIAA.
[2] Full Professor, Faculty of Aerospace Engineering, Delft University of Technology, Member AIAA.
[3] Associate Professor, Faculty of Aerospace Engineering, Delft University of Technology.

T = time taken for one flapping cycle
u_i = Cartesian velocity components
U_∞ = freestream velocity
x_i = Cartesian coordinates
x_{13} = horizontal distance between the trailing edge of fore airfoils and the leading edge of the tail, nondimensionalized by airfoil chord
y_{12} = vertical distance between the top and bottom airfoil at their closest position, nondimensionalized by airfoil chord
y_{13} = vertical distance between the symmetry line and the leading edge of the tail, nondimensionalized by airfoil chord
α = angle of attack of the tail, measured clockwise along the horizontal, in degrees
ϕ = phase difference between pitching and heaving, in degrees
ρ = density of fluid
θ = instantaneous pitch angle, in degrees
θ_0 = pitch amplitude, in degrees
η = propulsive efficiency
v_c = space-averaged streamwise velocity at the exit

I. Introduction

Flapping wing micro-aerial vehicles (FMAVs) have become increasingly popular, especially in the area of military and civilian surveillance. They exhibit excellent maneuverability and efficiency at this low Reynolds number (*Re*) regime. Besides the traditional FMAVs which have a single pair of wings[1] similar to birds, other variations exist as well. One of these is our Delfly[2,3], which features a biplane wing design. During the design of the Delfly, three ornithopter configurations were studied – the simple monoplane with one set of wings, the biplane design where two sets of wings were placed above each other moving in counter phase, and a tandem configuration where two wings were placed one behind the other. The biplane was finally selected due to its low power requirement and zero rocking amplitude[3].

Another variation is the FMAV designed by Jones and Platzer[4], which has a fixed wing for lift and two flapping wings in a biplane configuration at the tail for thrust. In this case, the biplane design stems from the study that an oscillating foil placed in the boundary layer of a flat surface generates a much stronger jet flow compared to one placed outside the free-stream. Numerical simulation by panel codes and experiments conducted further confirmed the improved thrust and propulsive efficiency. Hence the most promising FMAV design is a closely coupled fixed-wing/oscillating biplane configuration. The biplane airfoils downstream of the fixed wing adds the favorable wake ingestion effect[5].

Tuncer and Kaya[6,7] have performed a number of studies on flapping biplane configurations. In their first study[6] , they use overset grids to simulate unsteady viscous flow over flapping airfoils in a biplane configuration using a Reynolds-averaged Navier-Stokes (RANS) solver. The biplane configuration produces up to 40% more thrust than a single (flapping) airfoil. The phase angle between the pitch and plunge oscillations of the airfoil has an important role on the flow development and thrust generation. The authors[7] next use a gradient based optimization process to try to obtain the maximum possible thrust production. The maximum pitch angle, plunge amplitude and phase angle are taken as the optimization variables. It was found that at low flapping frequency, the biplane configuration produces more thrust than a single airfoil. However, at high frequency, the pitch amplitude tends to zero, promoting early leading edge vortex (LEV) formation and limiting the thrust production.

Miao, Sun and Tai[8] simulated flow past a biplane flexible airfoil configuration using FLUENT. They tested airfoils with different prescribed flexibility and found that at a flexure extent of 0.25 time the chord length, propulsive efficiency is maximum and 65% more than that of biplane rigid airfoils. Moreover, the thrust power coefficient is influenced primarily by the value of the reduced frequency (range between 0.5 to 3.5) rather than the Reynolds number (range between 10^2 to 10^4).

The current research is an extension of an earlier study, which studies on the interference effect between a single flapping airfoil and the stationary tail in a tandem configuration. The current study aims to investigate the effect of the biplane airfoils and its tail on the efficiency (η), average thrust ($\overline{C_t}$) and lift ($\overline{C_l}$) coefficient. The present investigation differs from the previous studies[4,6-8] in that now a tail is included. Moreover, the focus of earlier studies was on the flapping parameters, rather than relative positions of the airfoils and tail. An Immersed Boundary Method (IBM)[9] Navier-Stokes solver[10] is used for the simulations. The motivation for adopting this approach is

discussed in more detail in the following section. The *Re* number used is 1000, which will help to limit the grid requirements as the non-conformal grid of the IBM requires a very high resolution grid. This Re value corresponds to the range of insects' flight and small MAVs. The results will be beneficial to the further improvement of the Delfly.

II. Numerical Method

The unsteady viscous flow fields are computed by solving the non-dimensional laminar Navier–Stokes equations using the IBM. Due to the biplane arrangement of the front airfoils and tail behind, it is difficult to use conforming grids with Arbitrary Lagrangian–Eulerian (ALE) formulation since maintaining grid quality can be a challenge, especially when the distance between the airfoil and tail is very small. The overset grid solver is a viable choice but stability and conservation problems may arise[9]. The IBM used in this research is based on the scheme by Ravoux et al.[10]. This method combines features from both the IBM and the volume of fluid (VOF) method in order to compute flows past moving and deformable bodies. The Ravoux scheme is chosen over the other IBM schemes because it is simple to implement. There is also no ad-hoc computation required such as the "freshly cleared cells" problem[11] when the body starts to move.

Similar to other IBM methods, an external body force density (*fc*), which signifies the presence of the solid body, is inserted into the fluid equations. The main idea is to consider the computational domain as a continuous fluid medium, which encompasses both the fluid and the body phase. The volume fraction of the rigid body phase is unity whereas that of the ordinary fluid phase has a volume fraction of zero. In the cells corresponding to the body-fitted interface, the medium is partially made up of the fluid and rigid body phases and volume fraction has a value between zero and unity. The force coefficient of the body can be obtained by satisfying the criteria that the velocity in the cells occupied by the solid must equal the velocity of the rigid body. We currently use a fully implicit scheme instead of the original fully explicit scheme to improve the stability of the solver. The unsteady flow results are analyzed in terms of efficiency, thrust, lift coefficients, while the flow behavior is visualized with the help of vorticity contour plots. The discretization and the time advancement scheme are discussed in the next section. More details about the solver and its verification and validation at *Re* = 1000 can be found in Ref. 10 and 12.

A. Fractional step method

A fractional step method, which is based on an improved projection method[1,3], is used to solve the modified non-dimensional incompressible Navier-Stokes equations (which has the external body force *fc* added) in Eq. (1) and (2).

$$\nabla \cdot u = 0\,, \tag{1}$$

$$\frac{\partial u}{\partial t} = -u \cdot \nabla u + \frac{1}{\mathrm{Re}} \nabla^2 u - \nabla p + fc \tag{2}$$

where u is the velocity, t is the time, p is the pressure, fc is the external body force, Re is the Reynolds number.

A fully implicit scheme which uses the Crank Nicholson approximation for the viscous term and convective term is employed to improve the stability of the solver. All spatial derivatives are discretized using the second-order central difference scheme on a staggered grid.

B. Computational domain

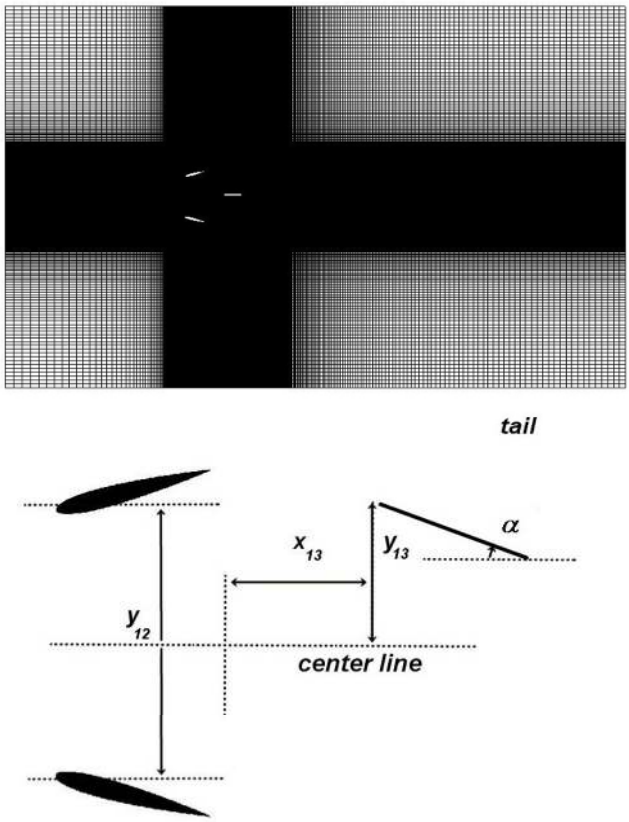

Figure 1 An example of the 1320×1120 Cartesian grid and its magnification

Two NACA0012 airfoils are placed in a biplane configuration for the first phase of the simulation. In the subsequent phase, a thin plate tail is placed behind the two airfoils. The 2D computational domain is discretized using a Cartesian grid. The domain size is 26 x 16 units, where one unit corresponds to the airfoil chord. The distances of the top/bottom and farfield downstream boundary to the airfoil are 8.0 and 17.5 units respectively. The grid resolution is 1320×1120 cells; refinement is used in the region near the airfoils. Figure 1 shows the grid and the parameters involved in this study. y_{12} is the vertical distance between the top and bottom upstream airfoils when they are at their closest plunging locations. x_{13} is the horizontal distance between the trailing edge of the front airfoil and the tail. y_{13} is the vertical distance between the center line and the tail's leading edge. α is the (constant) incidence angle of the tail. The upstream top airfoil's flapping motion is specified by

$$h = h_0 \sin(2\pi f (t - t_0) - \phi), \qquad \theta = \theta_0 \sin(2\pi f (t - t_0)) \tag{3}$$

The upstream bottom airfoil's flapping motion is the mirror image of the top airfoil's. The downstream airfoil is stationary and simulates the tail of the airfoil. The pitching motion is about the quarter chord point. The phase angle ϕ is 90^o in all simulations, so that the pitch and heave are one quarter period shifted in phase.

C. Boundary conditions

The boundary conditions prescribed on the domain boundaries are :

Inflow boundary - $u_x = U_\infty = 1$, $u_y = 0$, $dp/dx = 0$

Top/bottom boundary – $u_y = 0$, $du_x/dy = 0$, $dp/dy = 0$

Outflow boundary - $\frac{\partial u_i}{\partial t} + v_c \frac{\partial u_i}{\partial x} = 0$, where v_c is space-averaged streamwise velocity at the exit[14], $p = 0$

where the subscript i refers to the x and y directions.

III. Results and Discussions

In this study, the objective is to investigate the effect of the relative distances y_{12}, x_{13}, y_{13} and the tail's angle of attack α on the overall efficiency, thrust and lift. The simulations consist of two phases. The first phase involves only the biplane wing and y_{12} is varied from 0.122 to 1.0. This phase focuses on determining the effect of y_{12} on the outputs. Based on the results from the first phase, two values of y_{12} which exhibit strong biplane wing effect will be chosen. The second phase of the simulation will make use of the y_{12} found and involve the tail too. x_{13} and α will range from 0.001 to 2.0 and -15° to 45° respectively. It is found that beyond x_{13} = 2.0, the effect of the tail on the overall η, C_t and C_l is negligible. In the third and last phase, the tail is shifted vertically by varying y_{13}.

The upstream NACA0012 airfoils flap with a prescribed motion. The Strouhal number St and the reduced frequency k are fixed at 0.2 and 0.4 respectively to isolate the effects of x_{13} and α. Moreover, these particular values are chosen because previous simulation results[15] showed that using too low values resulted in little or no shedding of vortex. This is because the energy input is too low. Tuncer[16] also observed this when low k and h_o are used. On the other hand, high St and k may result in chaotic vortex shedding. This will hinder a systematic analysis of the effect of x_{13} and α. A description of the motion parameters for the detailed flapping configuration is given in Table 1. The single airfoil is simulated under the same flapping configuration for comparison.

Table 1 Flapping configuration

Re	1000
St	0.2
k	0.4
ϕ / degrees	90.0
θ_0 / degrees	17.5
y_{12}	0.122 – 1.0
x_{13}	0.001 – 2.0
α / degrees	-15.0 – 45.0

In this study, the power input of an airfoil is defined as

$$P_{in} = -L(t)\frac{dh}{dt} - M(t)\frac{d\theta}{dt} \tag{4}$$

Propulsive efficiency, η, which is a measure of the energy lost in the wake versus energy used in creating the necessary thrust, is given by

$$\eta = \frac{Thrust.U_\infty}{\overline{P}_{in}(\text{dimensional})} = \frac{\overline{C}_t}{\overline{P}_{in}} \tag{5}$$

A. Biplane tail-less configuration: Effect of y_{12}

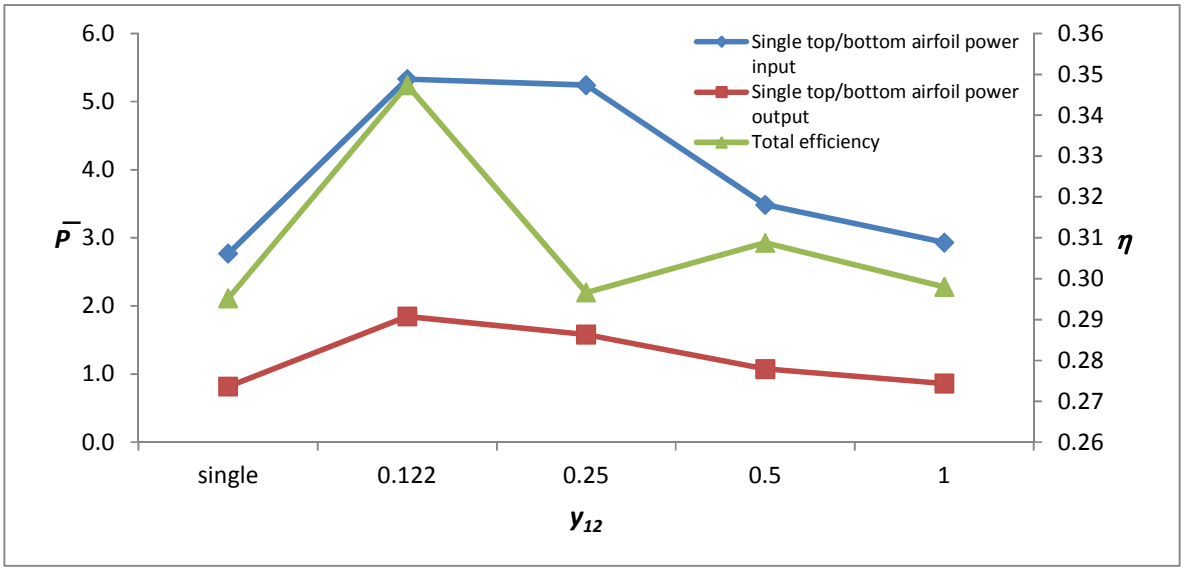

Figure 2 Plot of η, $\bar{P}_{in}$ and $\bar{P}_{out}$ C_t against y_{12}, $\alpha = 0^o$

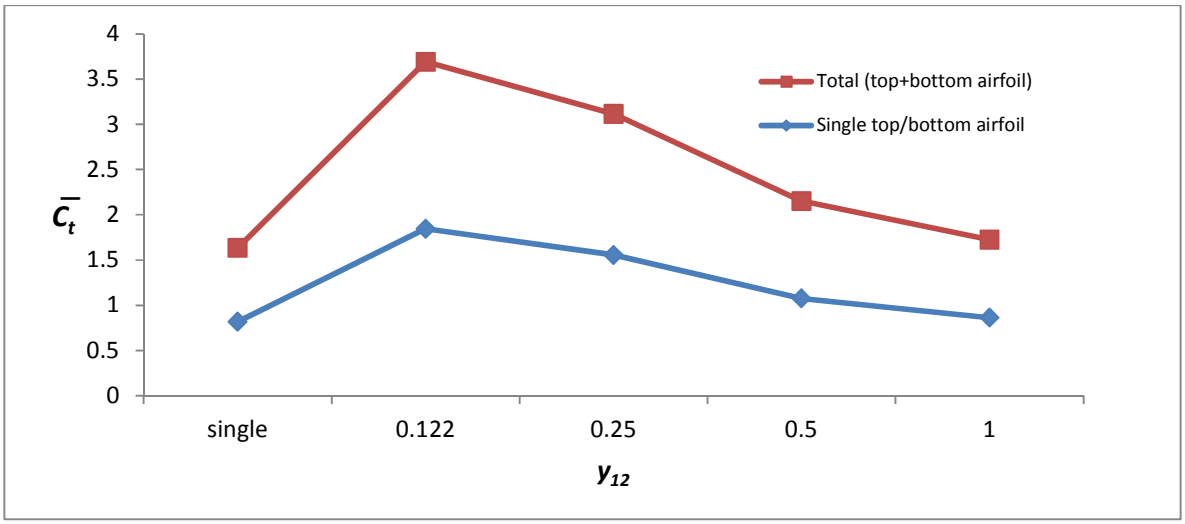

Figure 3 Plot of $\bar{C}_t$ against y_{12}, $\alpha = 0^o$

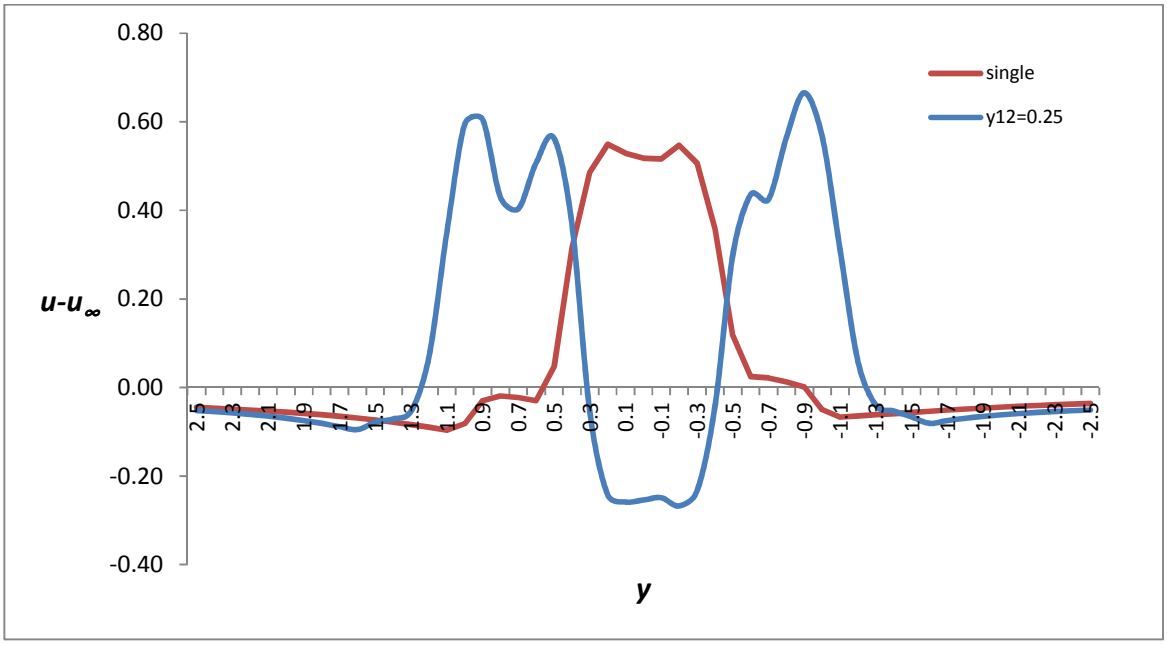

Figure 4 Average velocity profile for the single airfoil and the y_{12} = 0.25 case

Figure 2 and Figure 3 show the efficiency (η) and average thrust coefficient ($\overline{C_t}$) for the single airfoil* and the biplane airfoils at different y_{12}. Because of the symmetrical configuration in this case, the top and bottom airfoils provide almost the same amount of thrust, equal to half of the total thrust. The maximum $\overline{C_t}$ for the top or bottom airfoil is 1.85 for the y_{12} = 0.122, which increases by an impressive 126% compared to the single airfoil case. The velocity profile in the wake of the wings depicted in Figure 4 shows that the area covered by the y_{12} = 0.25 case is about twice that of the single airfoil case, indicating the high thrust created by the biplane arrangement. The high thrust has also been observed in Ref. 4 and 6 although the flapping parameters are different and their simulation were mostly performed at $Re = 10^4$. Miao, Sun and Tai[8] also did a sub-study comparing thrust at $Re = 10^3$ and 10^4 and found that they are very similar.

* Total $\overline{C_t}$ for the single airfoil is defined as twice the thrust produced by the single individual airfoil. This ensures a fair comparison.

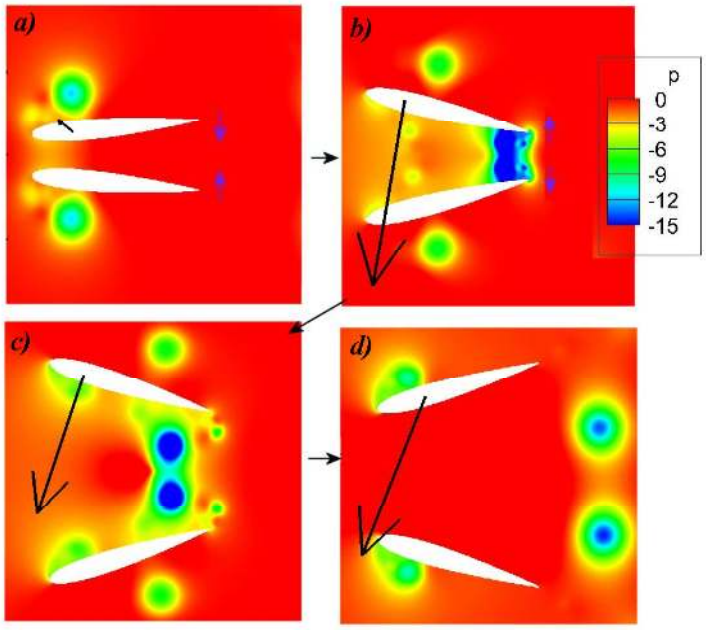

Figure 5 Pressure contour plots of the y_{12} = 0.25 case

1. Thrust

Figure 5 shows the pressure contour plots of the y_{12} = 0.25 biplane case during different phases of the flapping cycle. The black and purple arrow indicate the non-dimensional instantaneous force vector on the top airfoil and the motion of the airfoils respectively. The force vector on the bottom airfoil is symmetrical to the top airfoil's with respect to the center horizontal line and it is not shown. Initially, pressure in the region between the top and bottom airfoils is approximately 0 units (the pressure is approximately equal to the free stream value, as shown in Figure 5a by the red color). As the distance between the two airfoils gets smaller, the pressure in the region decreases, especially near the airfoils' trailing edge, evident from the deep blue color contour. When the airfoils separate, this low pressure region creates a high thrust, resulting in the shedding of two vortices. This is different from the wing-in-ground (WIG) effect which a stationary airfoil experiences when it is near to a surface. In that case, the result is the increased lift due to the higher pressure throughout the lower region of the airfoil. However in the current flapping airfoils, the pressure in the region in between the two airfoils becomes lower, especially so around the airfoils' trailing edges. It gives an overall increase in thrust instead of lift. Although the instantaneous lift can be very large (as high as C_l = 11.2 as shown by the black vector arrow), the instantaneous lift from the top and bottom airfoils cancelled out since their C_l are in the opposite direction.

At y_{12} = 0.122, which is the case where the top and bottom airfoils almost touch (0.002c apart), a slightly different phenomenon is observed. As shown in Figure 6, for the y_{12} = 0.25 case, the vortices remain attached to the trailing edge of the airfoils. On the other hand, for the y_{12} = 0.122 case, when the top and bottom airfoils almost touch, the two trailing vortices are forced to come into contact with one another and shed as a result. A strong jet is seen spurting out. This is not seen in the y_{12} = 0.25 case. Hence, when two airfoils come into contact, the trailing vortices have to shed and this creates an even higher thrust. Simulating y_{12} = 0.122 with the top and bottom airfoils almost touching poses no problem because the IBM solver is used. It is much more difficult for other biplane studies[6-8] which use overset and conformal hybrid grids to accomplish this.

This wings-touching interaction has also been experimentally observed in our FMAV Delfly, whereby its wings also come into contact with each other[17]. This has been identified as the clap-and-peel mechanism[18]. The recorded in-flight wing deformation showed that during the start of the out-stroke, the flexible biplane wings peel apart at the leading edge, while they clap together at the trailing edge. This peeling of the wings creates a rearward directed flow and the clap of the wings creates a rearward momentum jet. The simulation is slightly different from the Delfly case in that rigid airfoils are used instead of membranes. Moreover, the motion of the airfoils is prescribed rather than the result of fluid structure interaction. Despite these facts, the thrust increase due to the momentum jet is found in both cases.

2. Efficiency

On the other hand, the increase in η is much lower compared to that of $\overline{C_t}$, up to a maximum of 20% at y_{12} = 0.122, as seen from Figure 2. At other values of y_{12}, the increase is either very small or none at all. Figure 2 shows the plot of the average power input $\overline{P}_{in}$ and output $\overline{P}_{out}$ for the different cases. $\overline{P}_{out}$ increases gradually as y_{12} decreases due to the corresponding increase in thrust. But $\overline{P}_{in}$ also increases, resulting in similar values of η for y_{12} between 0.25 and 1.0. The reason for the increase in $\overline{P}_{in}$ is due to the larger instantaneous lift force, as a result of higher pressure difference between the top and bottom side of the airfoils. This phenomenon is similar to the wing-in-ground (WIG) effect. However, at y_{12} = 0.122, when the top/bottom airfoils almost touch, the pressure between these two airfoils does not increase further. Therefore, the $\overline{P}_{in}$ for the y_{12} = 0.122 and 0.25 are similar. With a higher $\overline{P}_{out}$ for the y_{12} = 0.122 case, its resulting η is higher.

Another interesting feature is the entanglement pairing of the vortices for the y_{12} = 0.5 case. It can also be seen for the y_{12} = 1.0 case but it is less obvious. Taking the top airfoil as reference, the trailing edge vortex remains attached for a much longer period compared to cases at y_{12} < 0.5. The shed leading edge vortex (LEV) "rolls" along the airfoil's surface and coincides with the shedding of the trailing edge vortex, resulting in the interaction. They entangle together and rotate as a whole. The same entanglement and rotation happens to the vortices shed by the bottom airfoil.

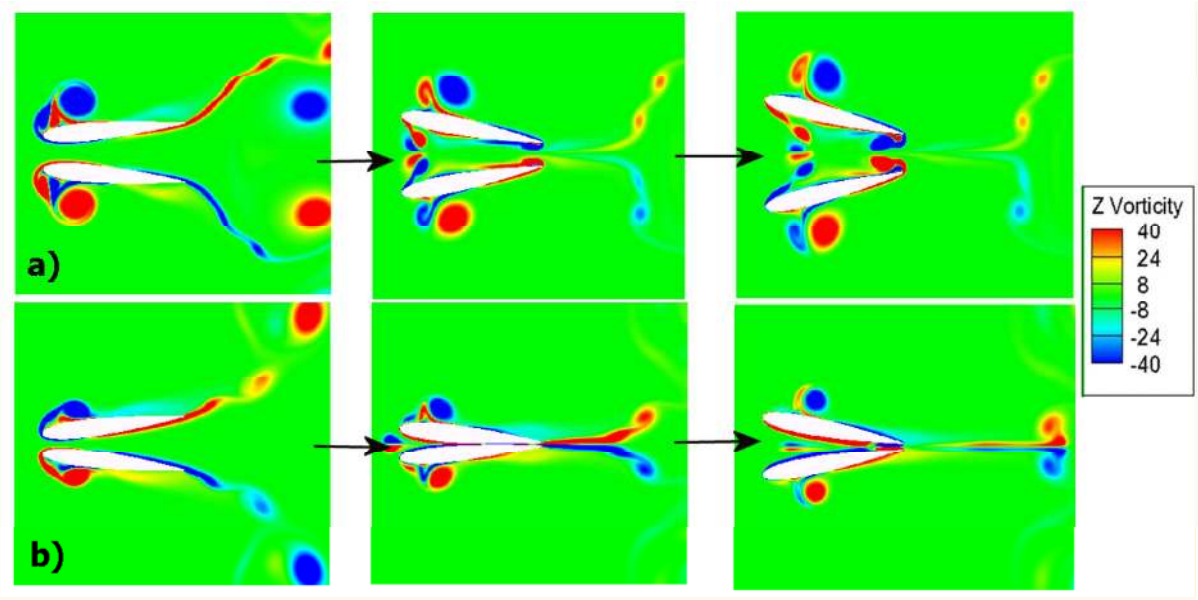

Figure 6 Vorticity contour plot of the a) y_{12} = 0.25 and b) 0.122 cases

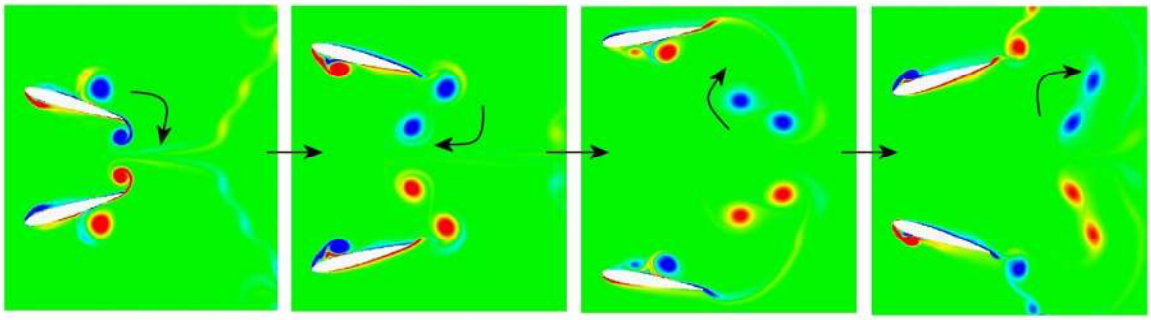

Figure 7 Vortex entanglement at y_{12} = 0.5

B. Biplane-tail configuration: Effect of total distance x_{13} and y_{13}

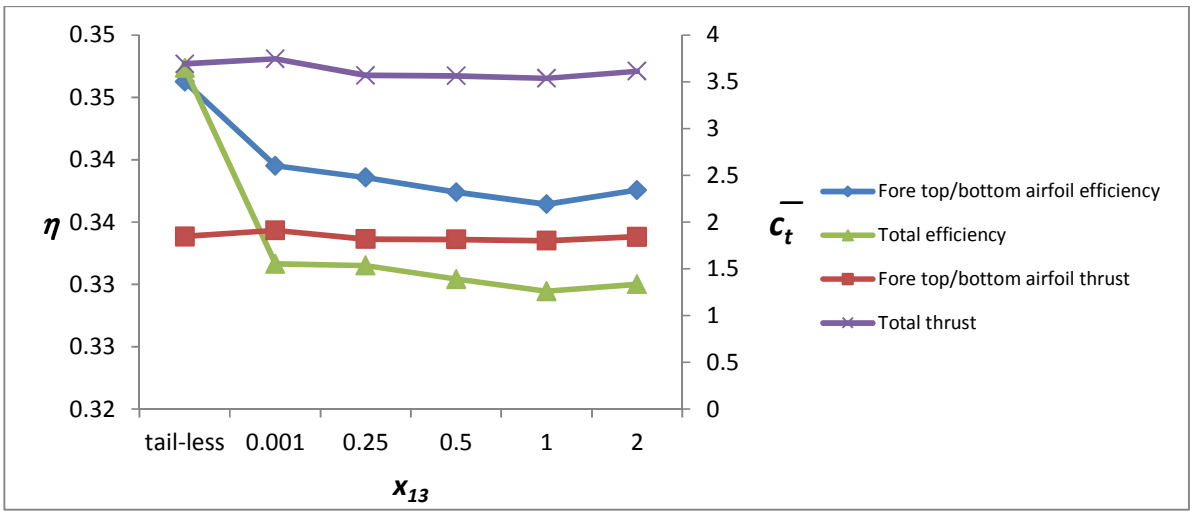

Figure 8 Plot of η, $\bar{C}_t$ against x_{13} at $y_{12} = 0.122$

In this section of the analysis, a tail is placed behind the biplane airfoils. The separation between the wings and the tail, x_{13} varies from 0.001 to 2.0. Regarding the biplane flapping motion, y_{12} is fixed at 0.122 and 0.25 because both are possible FMAV configurations and hence they are worth investigating more. However, not all results are shown. Only results of interests are discussed.

From the plot given in Figure 8, it can be seen that for the $y_{12} = 0.122$ case, varying x_{13} does not change the η and $\bar{C}_t$. In fact, by comparing with the tail-less configuration (also at $y_{12} = 0.122$), there is very little difference whether the tail is present or not. The vorticity plot in Figure 9 shows clearly that the shed vortices and the momentum jet pass through the tail as if it is not present since the location of the tail is along the symmetry line.

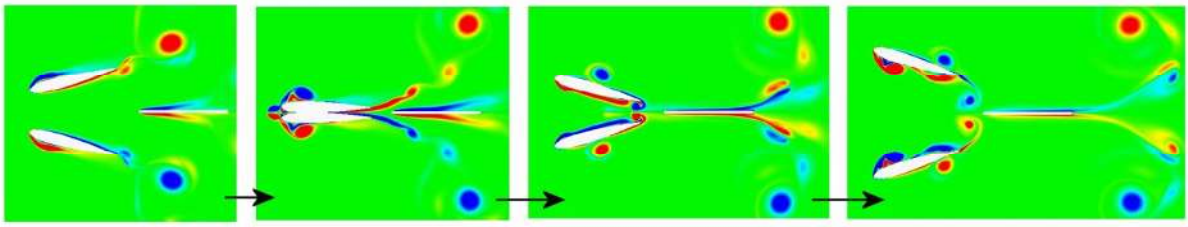

Figure 9 Vorticity plot of biplane with tail at $y_{12} = 0.122$ and $x_{13} = 0.25$

As a result, further investigation is carried out by shifting y_{13}, the vertical position of the tail to coincide with the mid plunge position of the fore top airfoil, which is the region where the vortices shed. In this case, y_{13} is taken to be 0.625. Figure 10 to Figure 12 shows the plot of η, $\bar{C}_t$ and $\bar{C}_l$ against x_{13} at $y_{12} = 0.25$ with $\alpha = 0^o$. The special case of $y_{13} = 0.625$ when $x_{13} = 1.0$ with $\alpha = 0^o$ is also included. Similar to the earlier $y_{12} = 0.122$ case, there is no difference in the η and $\bar{C}_t$ as x_{13} varies from 0.25 to 1.0. However, when the vertical location of the tail y_{13} is shifted to 0.625, there is a large change in the output. Although the thrust and efficiency of the flapping airfoils is not strongly affected, the overall performance of the complete airfoils-tail configuration is deteriorated because of the negative thrust contribution of the tail. This causes the $\bar{C}_t$ to drop from 3.1 to 1.5, and as a result η decreases from around 0.29 to 0.15. However, $\bar{C}_l$ increases from 0.0 to 3.75. The total $\bar{C}_l$ was initially close to zero at $y_{13} = 0.0$ because the positive lift generated by the fore bottom airfoil is cancelled out by the negative lift by the fore top airfoil. Lift generated by the tail was zero. The top three plots (a to c) in Figure 13 show the development of the LEV at the bottom of the tail. The vortex sheds in Figure 13b but soon after a second LEV develops which immediately interacts with the incoming vortex of the fore top airfoil and sheds. The bottom three plots (d to f) shows the development of the LEV at the top of the tail. The initial vortex also sheds but it stays close to the tail's

top. The secondary vortex which forms is much smaller but it did not shed until it reaches the trailing edge. In other words, the pressure at the tail's top is much lower than its bottom most of the time, resulting in the high lift. Moreover, the motions of the shed vortices from the fore airfoils were interrupted by the tail, reducing the overall thrust and efficiency. The position of the tail is therefore very important to the overall performance of a biplane FMAV. It can either give high thrust and efficiency or high lift.

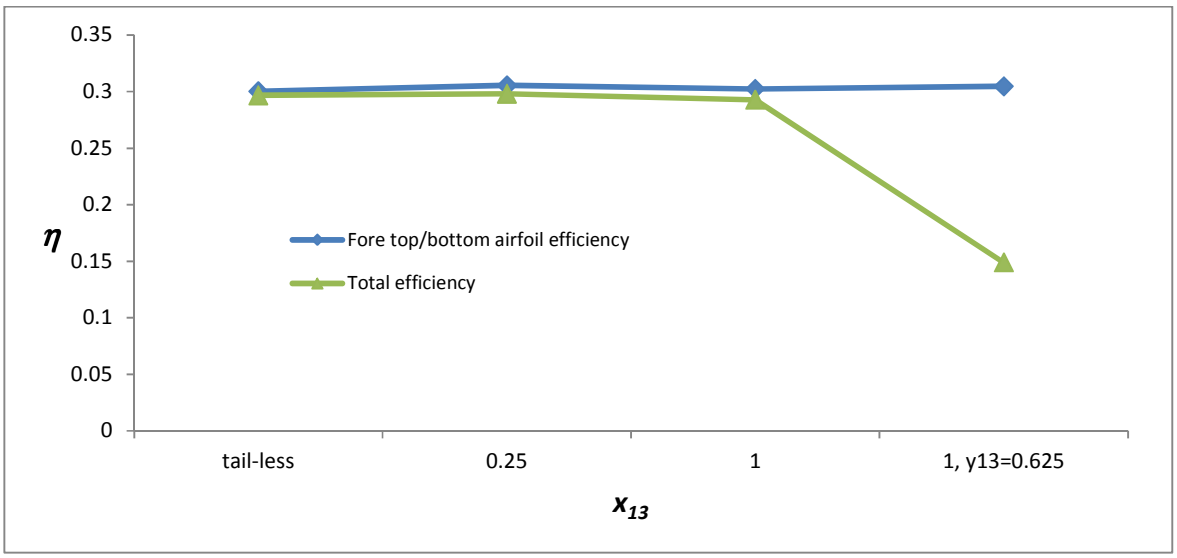

Figure 10 Plot of η against x_{13} at $y_{12} = 0.25$

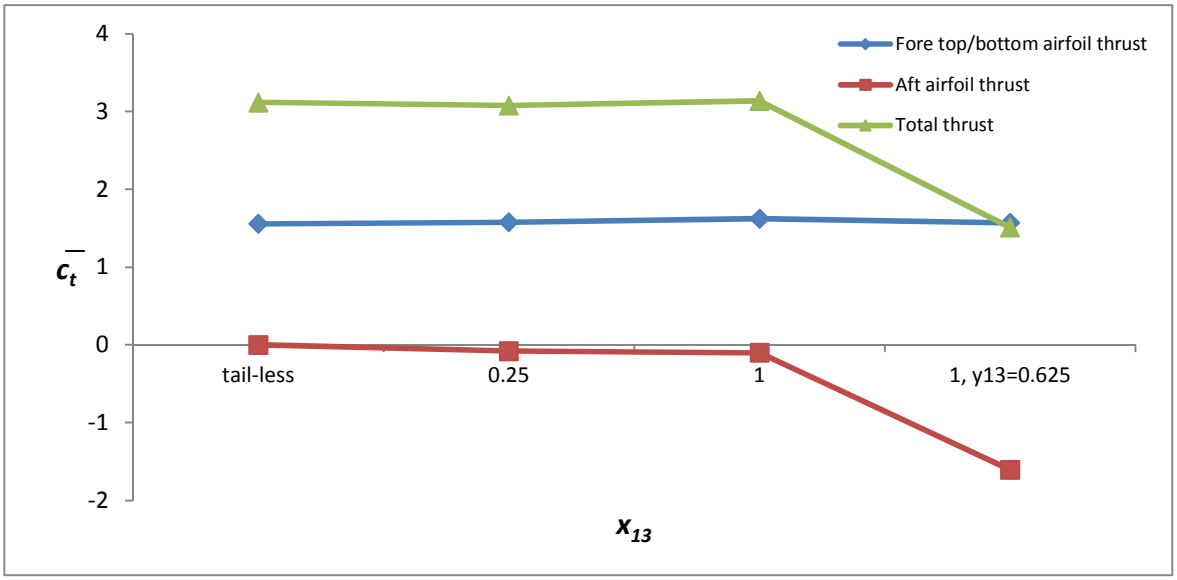

Figure 11 Plot of $\bar{C_t}$ against x_{13} at $y_{12} = 0.25$

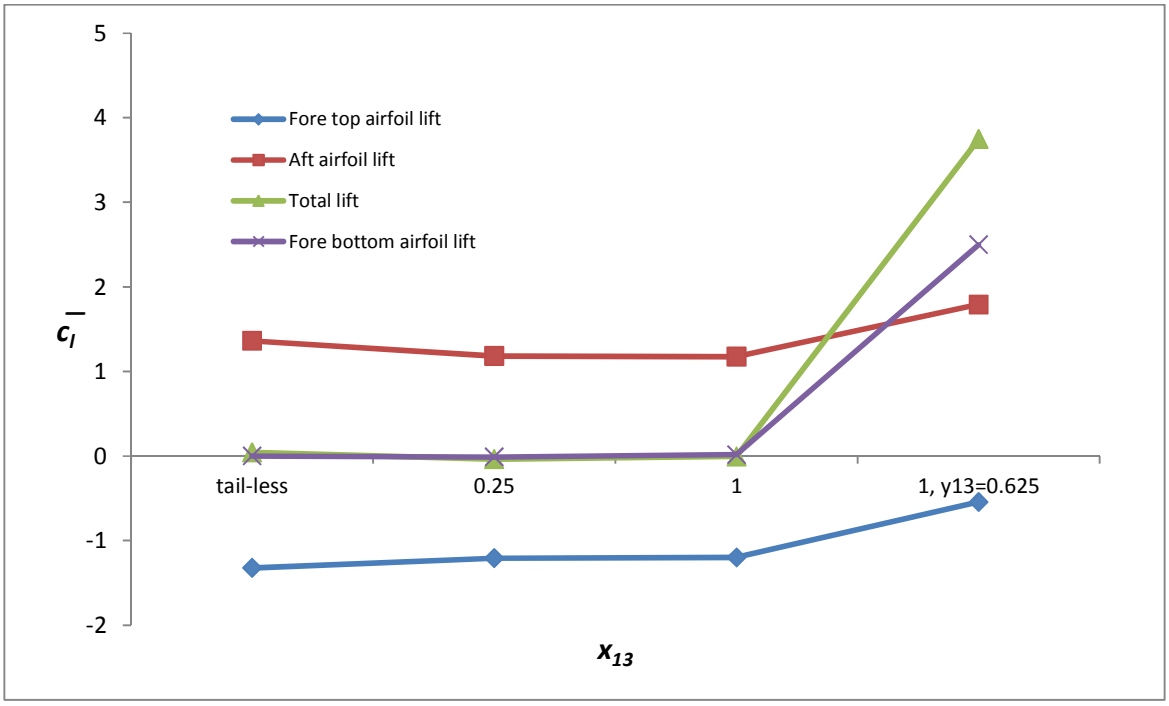

Figure 12 Plot of $\bar{C}_l$ against x_{13} at $y_{12} = 0.25$

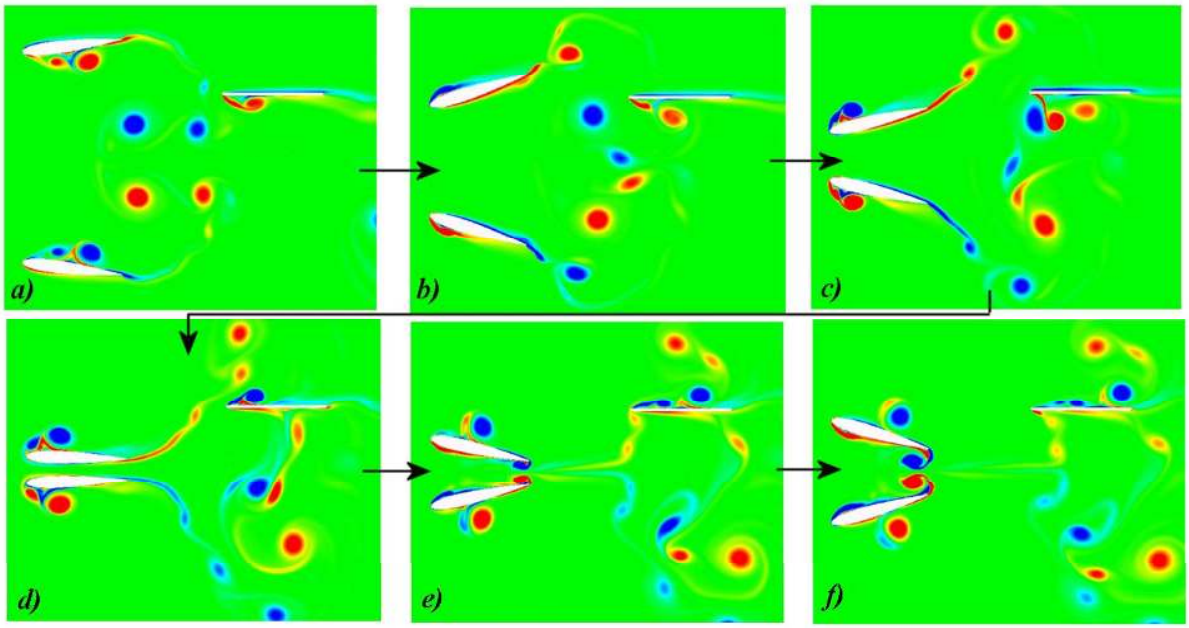

Figure 13 Vorticity plot of biplane with tail at $y_{12} = 0.25$, $x_{13} = 1.0$ and $y_{13} = 0.625$

C. Biplane-tail configuration: Effect of α and y_{13}

In this section, the objective is to determine the effect of α, the angle of the tail on the outputs. Figure 14 to Figure 16 show the variation of η, $\bar{C}_t$ and $\bar{C}_l$ against α at $y_{12} = 0.25$, $x_{13} = 1.0$ and $y_{13} = 0$. Both η and $\bar{C}_t$ drop when α deviates from zero. As α increases, $\bar{C}_l$ also increases. This is very similar to the results from the earlier

study involving the two airfoils tandem configuration (a single flapping airfoil in front and stationary tail directly behind)[19], albeit the change is much smaller.

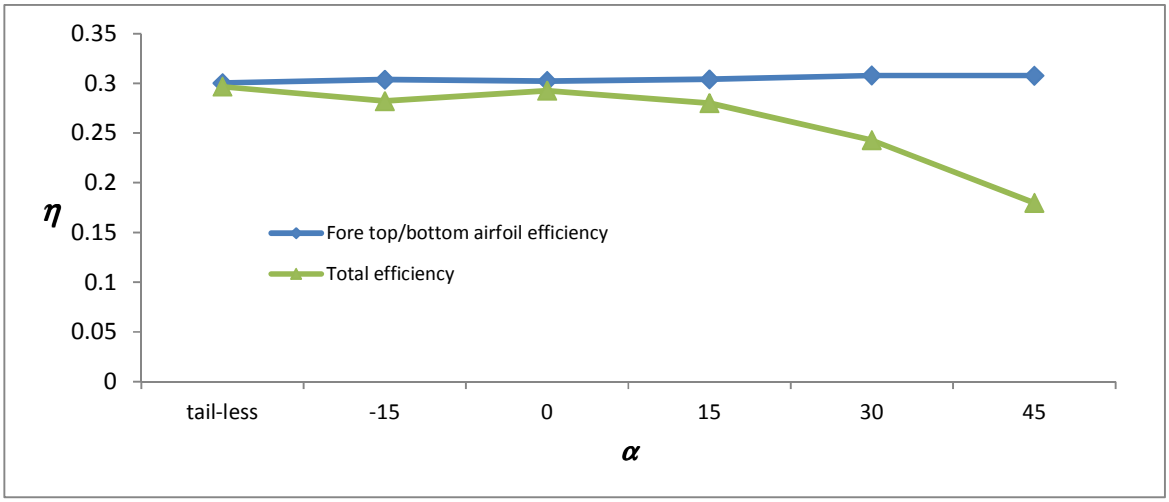

Figure 14 Plot of η against α at $y_{12} = 0.25$ and $x_{13} = 1.0$

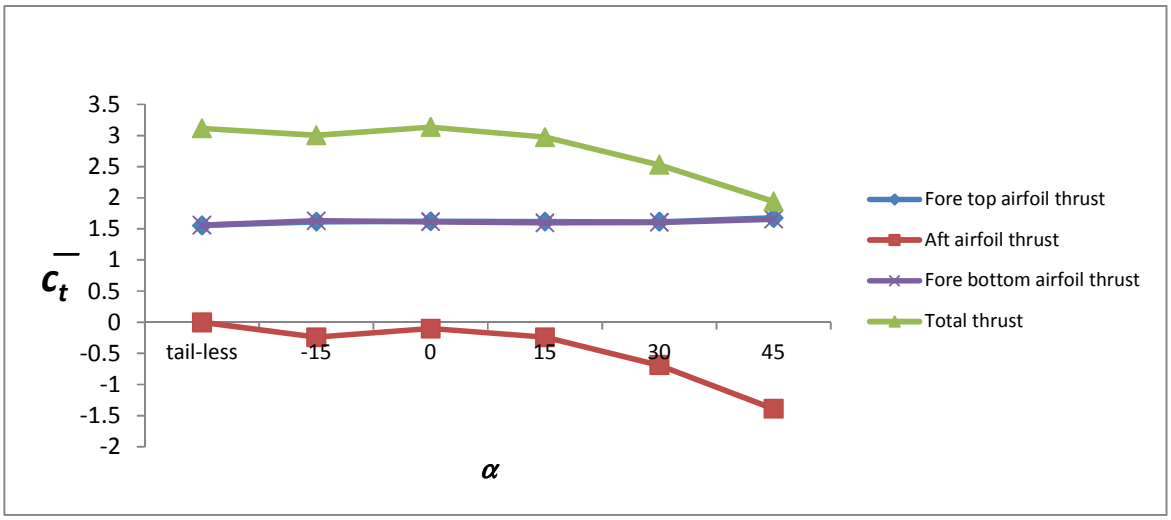

Figure 15 Plot of $\overline{C_t}$ against α at $y_{12} = 0.25$ and $x_{13} = 1.0$

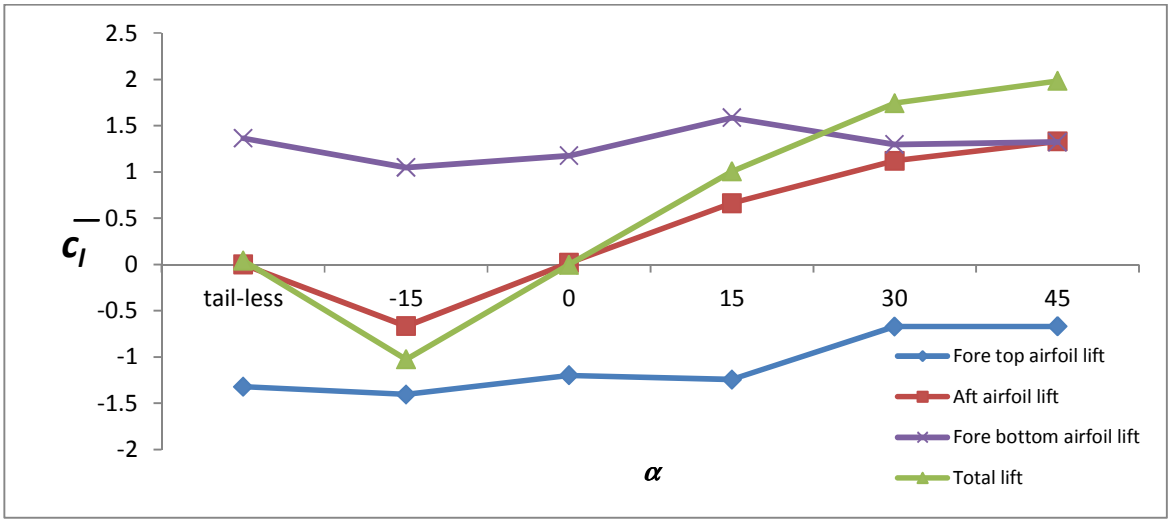

Figure 16 Plot of $\bar{C}_l$ against α at y_{12} = 0.25 and x_{13} = 1.0

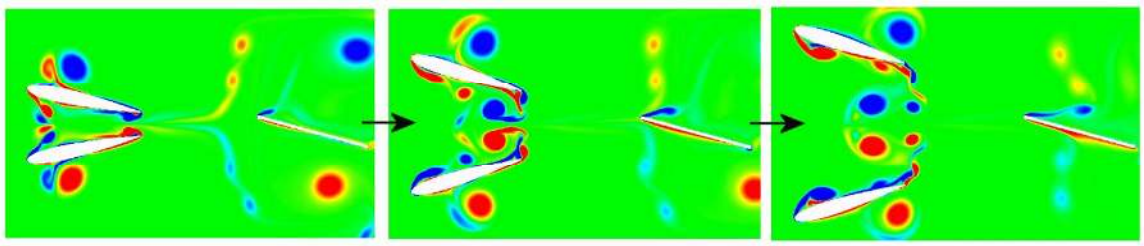

Figure 17 Vorticity plots at at y_{12} = 0.25, x_{13} = 1.0 and α = 15°

As shown in Figure 17, $\bar{C}_l$ increases due to the small LEV at the top of the tail, although in this case it is much weaker than the two airfoils tandem configuration[19] case. This results in a low pressure region on top the downstream airfoil, generating lift. The $\bar{C}_l$ (and therefore η) drops slightly because the tail has disrupted the vortices shed by the fore airfoils.

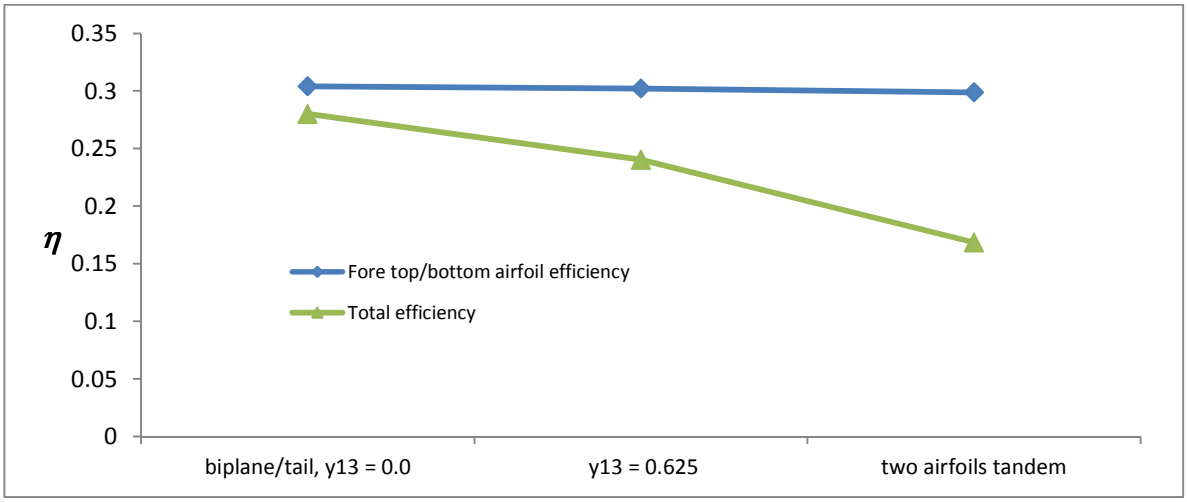

Figure 18 Plot of η of the biplane-tail arrangement at y_{12} = 0.25, x_{13} = 1.0, y_{13} = 0.0/0.625 and the two airfoil tandem arrangement at x_{13} = 1.0. α = 15°

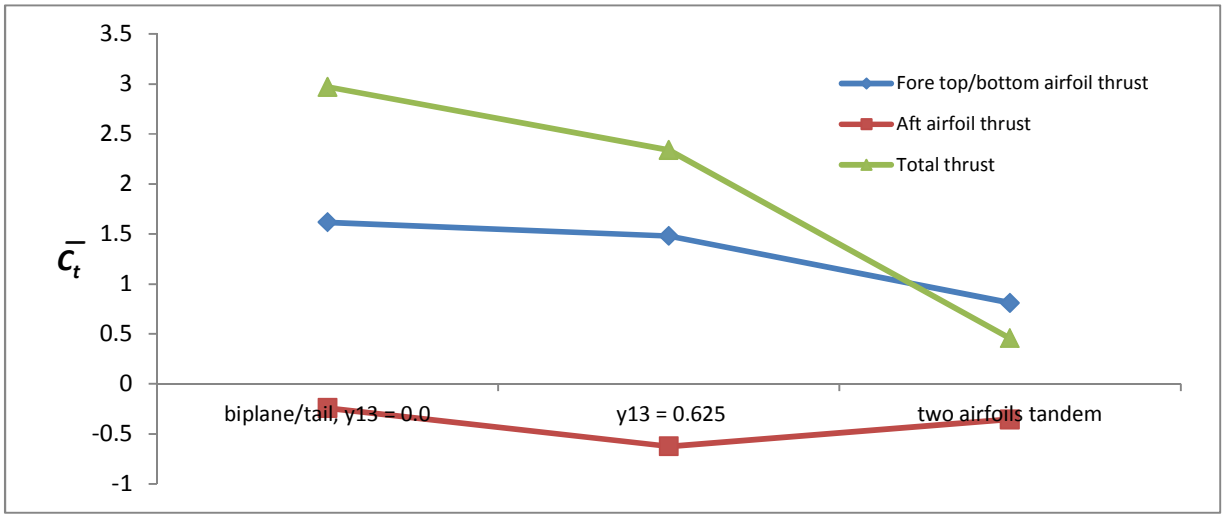

Figure 19 Plot of $\bar{C}_t$ of the biplane-tail arrangement at y_{12} = 0.25, x_{13} = 1.0, y_{13} = 0.0/0.625 and the two airfoil tandem arrangement at x_{13} = 1.0. α = 15°

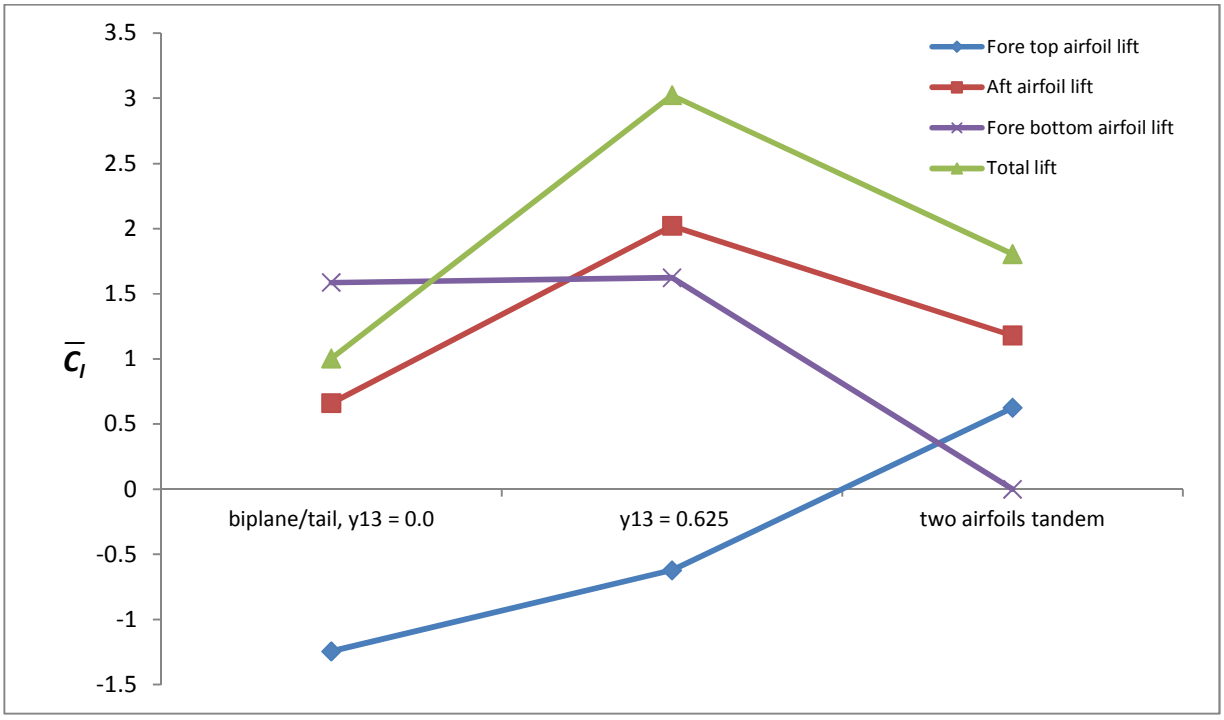

Figure 20 Plot of $\bar{C}_l$ of the biplane-tail arrangement at y_{12} = 0.25, x_{13} = 1.0, y_{13} = 0.0/0.625 and the two airfoil tandem arrangement at x_{13} = 1.0. α = 15°

The same simulation is repeated with y_{13} = 0.625. Figure 18 to Figure 20 show the η, $\bar{C}_t$ and $\bar{C}_l$ for the biplane/tail configurations at y_{13} = 0.0, 0.625 and the two airfoils tandem case[19]. When y_{13} = 0.625, its η and $\bar{C}_t$ is lower than the biplane/tail case but it is higher than the two airfoils tandem's. As for the $\bar{C}_l$, the y_{13} = 0.625 case performed the best. Figure 21 shows the comparison between the a) two airfoils tandem and b) biplane/tail cases. Only one LEV is formed at the top of the tail for the two airfoils tandem case. It sheds away after staying attached

for a short period of time. For the biplane/tail case, an even larger LEV forms at its tail's top. After this LEV sheds, a secondary smaller LEV forms again. Hence this explains the higher $\overline{C_l}$.

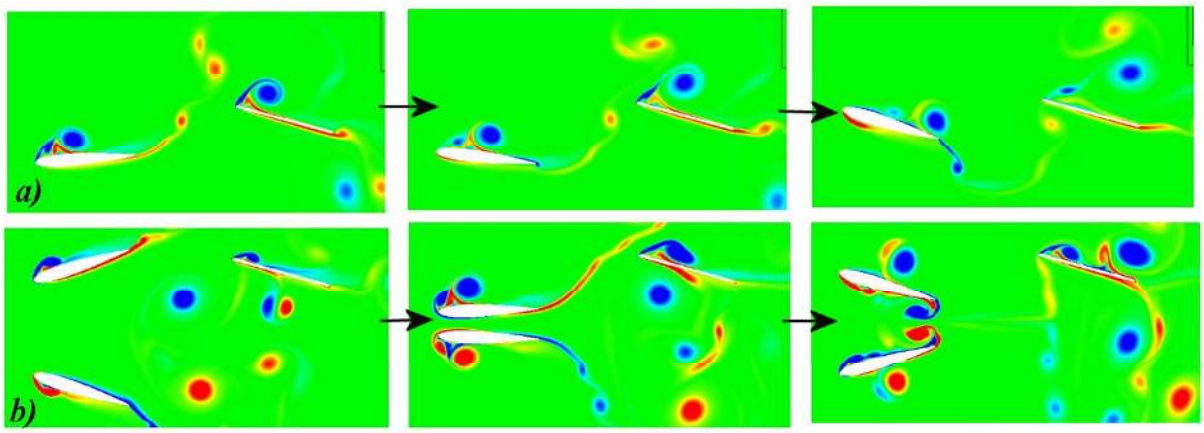

Figure 21 Vorticity plots of the a) two airfoils tandem b) and biplane/tail with y_{13} = 0.625 at x_{13} = 1.0 and α = 15°

IV. Conclusion

Numerical flow simulations have been performed out to investigate the effects of the y_{12}, x_{13}, α and y_{13} on the η, $\overline{C_t}$ and $\overline{C_l}$ in a biplane/tail configuration. In a biplane only configuration (without the tail), as the vertical distance y_{12} between the top and bottom airfoils decreases, the η and $\overline{C_t}$ increase, especially at y_{12} = 0.122, when the two airfoils almost touch. A strong jet spurts out, which is similar to what has been observed in our FMAV Delfly. It was then identified as the clap-and-peel mechanism[18]. Vortex entanglement has also been observed for the y_{12} = 0.5 and 1.0 cases.

Adding a horizontal tail into the simulation does not change the outputs if the tail is orientated along the symmetry line (y_{13} = 0.0; α = 0°). When y_{13} changes to 0.625, the mid plunge position of the top airfoil, the η and $\overline{C_t}$ drop to half of the original value but $\overline{C_l}$ increases to 3.75 due to the LEV developed on top of the tail.

The angle of the tail, α is then changed from zero to between -15° and 45°. Both η and $\overline{C_t}$ drop when α deviates from zero. As α increases, $\overline{C_l}$ also increases. When y_{13} = 0.625, a primary large LEV and a smaller secondary LEV are observed on the tail's top, resulting in a much higher $\overline{C_l}$.

These results showed that in a biplane/tail configuration similar to that of the Delfly[2], the different parameters have a great impact on the performance of the FMAV. By decreasing the distance between the top/bottom airfoils (y_{12}), more thrust can be produced. If higher lift is desired, the tail can be shifted upwards (increasing y_{13}) and the angle of the tail (α) be increased. In this research, no optimization study has been performed. Hence optimization study similar to those used by Kaya and Tuncer[7] can be used to further improve the η, $\overline{C_t}$ and $\overline{C_l}$ by varying the flapping parameters and relative distances between the airfoils and tail.

Acknowledgments

The work was carried out under support of the Dutch Technology Foundation (STW) under grant number 11023.

References

[1]Pornsin-sirirak, T., "Titanium-alloy MEMS wing technology for a micro aerial vehicle application," *Sensors and Actuators A: Physical*, Vol. 89, Mar. 2001, pp. 95-103.

[2]Groen, M., Bruggeman, B., Remes, B., Ruijsink, R., Oudheusden, B.W.V., and Bijl, H., "Improving flight performance of the flapping wing MAV DelFly II," *International Micro Air Vehicle Conference and Flight competition (IMAV 2010), Braunschweig*, 2010.

[3]Croon, G.C.H.E.D., Clercq, K.M.E.D., Ruijsink, R., and Remes, B., "Design, aerodynamics, and vision-based control of the DelFly," *International Journal of Micro Air Vehicles*, Vol. 1, 2009, pp. 71-98.

[4]Jones, K.D. and Platzer, M.F., "Design and development considerations for biologically inspired flapping-wing micro air vehicles," *Experiments in Fluids*, Vol. 46, Apr. 2009, pp. 799-810.

[5]Betz, A., *Introduction to the theory of flow machines*, Pergamon, New York, 1966.

[6]Tuncer, I.H. and Kaya, M., "Thrust generation caused by flapping airfoils in a biplane configuration," *Journal of Aircraft*, Vol. 40, 2003, pp. 509-515.

[7]Kaya, M., Tuncer, I.H., Jones, K.D., and Platzer, M.F., "Optimization of Flapping Motion Parameters for Two Airfoils in a Biplane Configuration," *Journal of Aircraft*, Vol. 46, Mar. 2009, pp. 583-592.

[8]Miao, J.-M., Sun, W.-H., and Tai, C.-H., "Numerical Analysis on Aerodynamic Force Generation of Biplane Counter-Flapping Flexible Airfoils," *Journal of Aircraft*, Vol. 46, Sep. 2009, pp. 1785-1794.

[9]Mittal, R. and Iaccarino, G., "Immersed Boundary Methods," *Annual Review of Fluid Mechanics*, Vol. 37, Jan. 2005, pp. 239-261.

[10]Ravoux, J.F., Nadim, A., and Haj-Hariri, H., "An embedding method for bluff body flows: interactions of two side-by-side cylinder wakes," *Theoretical and Computational Fluid Dynamics*, Vol. 16, 2003, pp. 433-466.

[11]Udaykumar, H.S., Mittal, R., Rampunggoon, P., and Khanna, A., "A sharp interface cartesian grid method for simulating flows with complex moving boundaries," *Journal of Computational Physics*, Vol. 174, 2001, pp. 345-380.

[12]Lim, K.B. and Tay, W.B., "Numerical analysis of the s1020 airfoils in tandem under different flapping configurations," *Acta Mechanica Sinica*, Vol. 26, Oct. 2009, pp. 191-207.

[13]Kim, D. and Choi, H., "A second-order time-accurate finite volume method for unsteady incompressible flow on hybrid unstructured grids," *Journal of Computational Physics*, Vol. 162, 2000, pp. 411-428.

[14]Pauley, L.L., Moin, P., and Reynolds, W.C., "The Structure of 2-Dimensional Separation," *Journal of Fluid Mechanics*, Vol. 220, 1990, pp. 397-411.

[15]Tay, W.B. and Lim, K.B., "Analysis of non-symmetrical flapping airfoils," *Acta Mechanica Sinica*, Vol. 25, 2009, pp. 433-450.

[16]Tuncer, I.H. and Platzer, M.F., "Thrust generation due to airfoil flapping," *AIAA Journal*, Vol. 34, Feb. 1996, pp. 324-331.

[17]Groen, M.A., "PIV and force measurements on the flapping-wing MAV DelFly II," M.Sc. Dissertation, Faculty of Aerospace Engineering, Delft University of Technology, 2010.

[18]Clercq, K.M.E.D., Kat, R.D., Remes, B., Oudheusden, B.W.V., and Bijl, H., "Flow visualization and force measurements on a hovering flapping-wing MAV 'DelFly II'," *39th AIAA Fluid Dynamics Conference*, Texas, 2009, pp. 1-10.

[19] Tay, W.., Bijl, H., and Oudheusden, B.W. van, "Analysis of tail effects in flapping flight," *International Micro Air Vehicle*, 't Harde, 2011.